

EFFECT OF ADIABATIC DECELERATION ON THE FOCUSED TRANSPORT OF SOLAR COSMIC RAYS

D. RUFFOLO

Department of Physics, Chulalongkorn University, Bangkok 10330, Thailand

Accepted for publication in the Astrophysical Journal

ABSTRACT

In the framework of focused transport theory, adiabatic deceleration arises from adiabatic focusing in the solar wind frame and from differential solar wind convection. An explicit formula is given for the deceleration of individual particles as a function of the pitch angle. Deceleration and other first-order effects of the solar wind, including convection, are incorporated into a numerical code for simulating the transport of energetic particles along the interplanetary magnetic field. We use this code to model the transport of solar flare protons. We find that including deceleration can increase the decay rate of the near-Earth intensity by 75% more than would be expected based on advection from higher momenta, due to an interplay with diffusive processes. Improved response functions are derived for the impulsive injection of particles near the Sun, and it is found that neglecting deceleration leads to incorrect estimates of the scattering mean free path based on the intensity decay alone, especially for lower-energy particles.

1. INTRODUCTION

The study of solar cosmic rays is marked by an incomplete understanding of the mechanisms for their acceleration and transport through the solar corona. One aspect of their behavior which is relatively well understood is their transport through the interplanetary medium. Because of this, one can attempt to perform numerical simulations of interplanetary transport, by which to deconvolve the measurements of solar cosmic rays by interplanetary spacecraft and derive their injection profile near the sun.

Recently, several authors have presented detailed numerical simulations of the focused transport of solar flare particles in the interplanetary medium (e.g., Earl 1976; Bieber 1977; Ng & Wong 1979; Kóta et al. 1982; Earl 1987; Ruffolo 1991; Pauls & Burger 1993). While these authors used a variety of numerical methods, they all treated particle transport in a framework in which particles follow helical orbits about the interplanetary magnetic field, subject to pitch-angle scattering and magnetic “focusing” or “mirroring”; we will refer to this as the framework of focused transport. These numerical studies have thus treated the particle distribution function, F , as depending on the time since the flare occurrence, t , the pitch-angle cosine, μ , and the distance along the interplanetary field, z .

One transport process which was not included in these previous treatments is that of adiabatic deceleration, although its effect on solar cosmic-ray distributions has been clearly demonstrated (e.g., Murray, Stone, & Vogt 1971). This process is commonly described as the adiabatic cooling of a isotropic cosmic ray “gas” in an expanding flow. It was proposed by Singer (1958) and Singer, Laster, & Lenchek (1962) that the deceleration of cosmic rays in expanding clouds of “magnetized solar plasma” could account for temporary Forbush decreases in cosmic ray intensity. Parker (1965) considered the expanding solar wind, and included the effects of deceleration, spatial diffusion, and convection in a Fokker-Planck equation for the cosmic ray distribution as a function of the radius and kinetic energy. Modified versions of this are still commonly used, e.g., in the study of solar modulation of galactic cosmic rays. Note that these treatments assume a nearly isotropic directional distribution.

On the other hand, Jokipii (1966) used a Fokker-Planck equation incorporating pitch-angle scattering and streaming to explain the cosmic ray distribution as a function of the distance along the magnetic field and the cosine of the pitch angle, which is defined as the angle between the particle’s velocity and the outward tangent to the average magnetic field. Once the effect of focusing was added (Earl 1976), this grew into the above mentioned framework of focused transport, which can explicitly model the anisotropy that is often observed in the cosmic ray distribution immediately after a solar flare event.

Thus for the most part, descriptions of solar cosmic-ray transport have included either momentum-changing solar wind effects (such as deceleration and convection) or pitch-angle dependent effects, but not both. Notable exceptions include the theoretical treatments of Skilling (1971, 1975), Luhmann (1976), Webb & Gleeson (1979), Earl (1984), and Schlickeiser (1989). To the author’s knowledge, no numerical simulations including both types of effects have been reported before.

In this work, we present an analytic treatment and numerical simulations of the interplanetary transport of energetic particles, including both anisotropic pitch-angle distributions and solar wind effects such as deceleration and convection. The latter are incorporated in the framework of focused transport, which already includes the former. After a description of adiabatic deceleration in this framework, and the derivation of explicit formulae for deceleration and other solar wind effects as a function of pitch angle, we present the equation of transport in a form which is suitable for numerical solution. We then describe a newly developed numerical code for the solution of this equation. As an application of the code, we examine the results of simulations of the interplanetary transport of solar cosmic rays. We find that the late-time decay due to “switching on” deceleration can be 75% faster than one would expect on the basis of momentum advection alone, because the advection rate is not spatially uniform, which enhances the decay rate due to spatial diffusion. Finally, we discuss possible future applications of the numerical method to the study of solar and galactic cosmic ray transport.

2. EQUATION OF TRANSPORT

2.1. *Adiabatic Deceleration*

Many studies of cosmic ray transport, particularly those concerning solar modulation, have used the formula

$$\langle \dot{p}' \rangle = -\frac{p'}{3} \nabla \cdot \mathbf{v}_{\text{sw}}, \quad (1)$$

where \mathbf{v}_{sw} is the solar wind velocity and p' is the particle momentum in the solar wind frame (Parker 1965; Dorman 1965). However, this average rate of deceleration is only valid when the particles’ pitch-angle distribution is nearly isotropic. In this section we relax this assumption, and consider the deceleration of individual particles as a function of the pitch angle. Our approach represents an extension of the focused transport model to include effects of the solar wind to first order in (v_{sw}/c) and examine those effects by means of numerical simulations; these effects have also been examined analytically in a more general context or to higher orders, e.g., by Luhmann (1976), Webb & Gleeson (1979), Earl (1984), and Schlickeiser (1989).

In the focused transport model (Earl 1976), energetic particles are considered to undergo pitch-angle scattering due to small-scale irregularities in the interplanetary magnetic field, and “focusing” or “mirroring” due to the large-scale divergence or weakening of the field at increasing distances from the sun. The latter process systematically decreases the pitch angle and increases μ , so that $v_{\parallel} = \mu v$ systematically increases, where v_{\parallel} is the component of the particle velocity moving outward from the sun along the local, average interplanetary magnetic field line. In this model the solar wind velocity is generally neglected. Both the large-scale and small-scale features of the field are treated as stationary, and the magnitude of the particle velocity is conserved by both focusing and scattering.

If, on the other hand, we do not neglect the solar wind velocity, we are led to consider two reference frames: the fixed frame and the local solar wind frame (comoving with the solar wind velocity at a given point). We denote particle velocities in these frames as \mathbf{v} and \mathbf{v}' , respectively, but for convenience we will always use the position in the fixed frame, following Jokipii & Parker (1970). Because the large-scale structure of the magnetic field is taken to be stationary in the fixed frame, the process of focusing conserves $v = |\mathbf{v}|$ (see Fig. 1a). Similarly, small-scale irregularities in the field can be considered to be frozen in the solar wind to a good approximation (Parker 1965). Then in the solar wind frame, the process of scattering conserves the magnitude of the velocity, $v' = |\mathbf{v}'|$.

2.1.1. *Radial Magnetic Field*

Now let us examine the effects of scattering and focusing as viewed in the solar wind frame (Fig. 1b). For simplicity, we first consider a radially-directed magnetic field with superimposed small-scale irregularities, assume a constant solar wind speed, and perform the velocity transformations non-relativistically. Scattering

preserves the magnitude of the velocity, v' , or the distance from the origin in the $v'_{\parallel} - v'_{\perp}$ plane. Thus scattering moves the velocity back and forth along semicircles centered at the origin (solid lines in Fig. 1b). Now the fixed frame moves at a velocity $-\mathbf{v}_{\text{sw}}$ with respect to this frame, as indicated by the point F in Fig. 1b; therefore, $\mathbf{v} = \mathbf{v}' + \mathbf{v}_{\text{sw}}$. Focusing preserves v , which is the distance from point F, and increases $v_{\parallel} = v'_{\parallel} + v_{\text{sw}}$. Thus this process moves the velocity to the right along semicircles centered at F (dotted lines in Fig. 1b); note that this is equivalent to the dB/dt effect in plasma physics. However, v' is not conserved, and in fact *systematically decreases* as focusing inevitably carries the particle velocity closer to the origin. As an example, Fig. 2 shows the schematic trajectory of a particle which alternately undergoes scattering and focusing, the latter of which always decreases v' .

The rate of deceleration for this example can be calculated in a straightforward way. Note that

$$\dot{v}' = \left. \frac{dv'}{d\mu} \right|_v \dot{\mu}. \quad (2)$$

The rate of change of μ in the fixed frame due to focusing, $\dot{\mu}$, is given by

$$\dot{\mu} = \frac{v}{2L(z)}(1 - \mu^2) \quad (3)$$

(Roelof 1969), where

$$\frac{1}{L(z)} \equiv -\frac{1}{B} \frac{dB}{dz}$$

and z is the arclength from the sun along the magnetic field. Substituting $\dot{\mu}$ into equation (2), evaluating the derivative, and simplifying, we find that

$$\dot{v}' = -\frac{v_{\text{sw}}v'}{2L(z)}(1 - \mu'^2).$$

A relativistic derivation yields a similar formula for the rate of change of the momentum (neglecting terms of order $(v_{\text{sw}}/c)^2$; normally $v_{\text{sw}}/c = 0.001$ to 0.002 near the Earth):

$$\dot{p}' = -\frac{v_{\text{sw}}p'}{2L(z)}(1 - \mu'^2). \quad (4)$$

For the radial field we are considering,

$$\frac{v_{\text{sw}}}{L(z)} = \frac{2v_{\text{sw}}}{r} = \nabla \cdot \mathbf{v}_{\text{sw}},$$

and therefore

$$\dot{p}' = -\frac{p'}{2}(1 - \mu'^2)\nabla \cdot \mathbf{v}_{\text{sw}}.$$

Then if the pitch-angle distribution in the solar wind frame is isotropic, the directional average of $1 - \mu'^2$ is $2/3$, and

$$\langle \dot{p}' \rangle = -\frac{p'}{3}\nabla \cdot \mathbf{v}_{\text{sw}}.$$

Therefore, the pitch-angle dependent formula, equation (4), yields equation (1) for the case of an isotropic pitch-angle distribution.

In the derivation presented above, adiabatic deceleration is a monotonic decrease in the momentum resulting from the transformation of adiabatic focusing from the fixed frame to the solar wind frame. However, adiabatic deceleration need not take place in a magnetic field; it would occur, for example, in a system of particles colliding with heavy “scattering centers” flowing away from the origin according to the velocity field, \mathbf{v}_{sw} (Gleeson & Axford 1967; Jones 1990). For this case, the motion of a particle between collisions is

along a straight line. However, since the orientation of \mathbf{v}_{sw} varies with position, the parallel component of the particle's velocity changes with time. Using spherical coordinates, we have

$$\dot{v}_r = \frac{v_\theta^2 + v_\varphi^2}{r},$$

or in terms of components parallel and perpendicular to \mathbf{v}_{sw} ,

$$\dot{v}_\parallel = \frac{v_\perp^2}{r}. \quad (5)$$

This kinematic effect is equivalent to adiabatic focusing (eq. [3]), because a magnetic field parallel to \mathbf{v}_{sw} does not affect v_\parallel . Thus adiabatic focusing (mirroring), or the increase in v_\parallel , can be viewed as a kinematical effect; the magnetic field merely serves to hinder the perpendicular motion. Equation (5), when transformed into the solar wind frame, then leads to adiabatic deceleration, whether or not a magnetic field is present.

2.1.2. Spiral Magnetic Field

So far, we have derived a pitch-angle dependent formula for the deceleration of a particle in a radial magnetic field. We now derive a similar formula for the case of an Archimedean spiral field. For convenience, we can use a fixed frame that is corotating with the sun, so that solar wind velocity, \mathbf{v}_{sw}^c , is parallel to the magnetic field at each point (Parker 1958). In particular,

$$\begin{aligned} \mathbf{v}_{\text{sw}}^c &= v_{\text{sw}} \hat{r} - \Omega r \sin \theta \hat{\varphi} \\ &= v_{\text{sw}}^c \hat{z}, \end{aligned}$$

and

$$v_{\text{sw}}^c = v_{\text{sw}} \sec[\psi(z)],$$

where Ω is the angular velocity of the solar rotation, \hat{z} is along the outward tangent to the average magnetic field, and $\psi(z)$ is the angle between \hat{r} and \hat{z} (see Fig. 3). Thus the corotating fixed frame and the local solar wind frame have a relative velocity \mathbf{v}_{sw}^c , and since this is parallel to the magnetic field, we can use the framework of the previous section (see Fig. 1).

As before, there is a systematic decrease in p' , the magnitude of the particle momentum in the solar wind frame, due to adiabatic focusing, as given by equation (4), replacing v_{sw} with v_{sw}^c . There is also an additional decrease due to changes in the solar wind velocity, v_{sw}^c , along the magnetic field. [These two effects are related to the perpendicular and parallel divergence of \mathbf{v}_{sw}^c , respectively, and were termed ‘‘betatron deceleration’’ and ‘‘an inverse Fermi effect’’ by Webb & Gleeson (1979).] Because of changes in \mathbf{v}_{sw}^c , the local solar wind frames are different at different locations; we call this effect ‘‘differential convection.’’ Consider a particle streaming from point A to point B on the same field line. We need to relate p'_A , the momentum in the local solar wind frame at point A, to p'_B at point B. Assuming a constant momentum in the fixed frame, and neglecting terms of order $(v_{\text{sw}}^c/c)^2$, we have

$$\begin{aligned} p'_{\parallel,A} &= p_\parallel - \frac{E}{c^2} v_{\text{sw},A}^c \\ p'_{\parallel,B} &= p_\parallel - \frac{E}{c^2} v_{\text{sw},B}^c \\ \Delta p'_\parallel &= -\frac{E}{c^2} v_{\text{sw}} (\Delta \sec \psi). \end{aligned}$$

If z is the arclength along the Archimedean field line, Δz is the distance from A to B, and Δt is the travel time, then

$$\begin{aligned} \Delta p'_\parallel &= -\frac{E}{c^2} v_{\text{sw}} \left(\frac{d}{dz} \sec \psi \right) \Delta z \\ &= -\frac{E}{c^2} v_{\text{sw}} \left(\cos \psi \frac{d}{dr} \sec \psi \right) v_\parallel \Delta t \\ \dot{p}'_\parallel &= -p_\parallel v_{\text{sw}} \left(\cos \psi \frac{d}{dr} \sec \psi \right). \end{aligned}$$

To examine the effect on p' due to differential convection alone, we can fix the value of p'_\perp . Since $p_\parallel v_{\text{sw}} = p'_\parallel v_{\text{sw}}$ to first order in (v_{sw}^c/c) , we find that the rate of deceleration due to changes in v_{sw}^c is

$$\begin{aligned}\dot{p}' &= \frac{p'_\parallel}{p'} \dot{p}'_\parallel \\ &= -p' v_{\text{sw}} \left(\cos \psi \frac{d}{dr} \sec \psi \right) \mu'^2.\end{aligned}\quad (6)$$

Finally, adding this rate of deceleration to that derived from equation (4) yields a total deceleration rate of

$$\dot{p}' = -p' v_{\text{sw}} \left[\frac{\sec \psi}{2L(z)} (1 - \mu'^2) + \cos \psi \frac{d}{dr} \sec \psi \mu'^2 \right], \quad (7)$$

which can again be shown to be equivalent to equation (1) for an isotropic pitch-angle distribution. Note that this expression for \dot{p}' is equivalent to that used by Skilling (1971).

2.2. Other Effects of the Solar Wind

Besides adiabatic deceleration, the solar wind velocity has other effects on the transport of solar flare particles. The effects described in this section are included in the transport code for the sake of completeness, although some of them represent rather small corrections for energetic particles. From now on we will continue to assume a constant, radial solar wind and an Archimedean spiral magnetic field.

One well-known effect is solar wind convection (e.g., Parker 1965). Since the distribution of particles tends to become isotropic in the solar wind frame due to pitch-angle scattering, solar wind convection can cause an anisotropy in the distribution observed in the fixed frame (the Compton-Getting effect; Compton & Getting 1935; Forman 1970). Comparing the parallel velocities in the fixed and corotating frames, we have

$$p_\parallel = \mu' p' + \frac{E}{c^2} v_{\text{sw}} \sec \psi,$$

and the rate of streaming is given by

$$\begin{aligned}\dot{z} &= v_\parallel = \frac{E'}{E} \mu' v' + v_{\text{sw}} \sec \psi \\ &= \mu' v' + \left(1 - \mu'^2 \frac{v'^2}{c^2} \right) v_{\text{sw}} \sec \psi,\end{aligned}\quad (8)$$

again neglecting terms of order $(v_{\text{sw}}^c/c)^2$ or higher.

In the standard focused transport model, the pitch-angle cosine in the fixed frame, μ , changes due to adiabatic focusing, as given by equation (3). In the local solar wind frame, this becomes

$$\begin{aligned}\dot{\mu}' &= \frac{d\mu'}{d\mu} \Big|_p \dot{\mu} \\ &= \frac{v'}{2L(z)} \left[1 + \mu' \frac{v_{\text{sw}}}{v'} \sec \psi - \mu' \frac{v_{\text{sw}} v'}{c^2} \sec \psi \right] (1 - \mu'^2),\end{aligned}\quad (9)$$

neglecting terms of order $(v_{\text{sw}}^c/c)^2$. Note the first-order correction factor in brackets.

In addition, μ' is affected by differential convection, i.e., changes in the solar wind velocity, v_{sw}^c . Equation (6) shows the contribution to \dot{p}' due to this effect. Since p'_\perp remains unaffected, we have

$$\begin{aligned}d(p'^2_\perp) &= 0 = d[p'^2(1 - \mu'^2)] \\ &= 2(1 - \mu'^2)p' dp' - 2\mu' p'^2 d\mu' \\ \dot{\mu}' &= \frac{1 - \mu'^2}{\mu'} \frac{\dot{p}'}{p'}.\end{aligned}$$

Using equation (6), we find that to first order in (v_{sw}^c/c) , the rate of change of μ' due to changes in v_{sw}^c is

$$\dot{\mu}' = -v_{\text{sw}} \left(\cos \psi \frac{d}{dr} \sec \psi \right) \mu' (1 - \mu'^2).$$

Combining this with the rate due to focusing, equation (9), we find that the total rate of change is

$$\begin{aligned} \dot{\mu}' = & \frac{v'}{2L(z)} \left[1 + \mu' \frac{v_{\text{sw}}}{v'} \sec \psi - \mu' \frac{v_{\text{sw}} v'}{c^2} \sec \psi \right] (1 - \mu'^2) \\ & - v_{\text{sw}} \left(\cos \psi \frac{d}{dr} \sec \psi \right) \mu' (1 - \mu'^2). \end{aligned} \quad (10)$$

2.3. Modified Equation of Focused Transport

In the previous sections, we considered the transport of particles in terms of the momentum in a frame comoving with the solar wind. Assuming that the large-scale structure of the field is stationary in a frame corotating with the sun, and that irregularities in the field are stationary in the local solar wind frame, we derived expressions for the rate of change of the momentum, p' , as a function of the pitch angle (eq. [7]), of z , the distance from the sun along the magnetic field (eq. [8]), and of μ' , the pitch-angle cosine (eq. [10]).

We now incorporate these expressions into a Fokker-Planck equation for the transport of energetic particles in the interplanetary magnetic field. Our equation is a modified version of those developed by Jokipii (1966) and Earl (1976), following the notation of Ng & Wong (1979). From now on, we will always be working with p and μ in the local solar wind frame, and for convenience, these variables are now written without primes. We start with a Fokker-Planck equation:

$$\begin{aligned} \frac{\partial F(t, \mu, z, p)}{\partial t} = & - \frac{\partial}{\partial z} \left(\frac{\Delta z}{\Delta t} F \right) - \frac{\partial}{\partial \mu} \left(\frac{\Delta \mu}{\Delta t} F \right) \\ & + \frac{\partial}{\partial \mu} \left[\frac{\varphi(\mu)}{2} \frac{\partial}{\partial \mu} \left(\frac{E'}{E} F \right) \right] - \frac{\partial}{\partial p} \left(\frac{\Delta p}{\Delta t} F \right), \end{aligned}$$

where $\varphi(\mu)$ is the pitch-angle scattering coefficient, the distribution function F is given by

$$F(t, \mu, z, p) = \frac{d^3 N}{dz d\mu dp},$$

and N represents the number of particles inside a given flux tube (Ng & Wong 1979). Note that there is a factor of $E'/E = 1 - \mu v v_{\text{sw}} \sec \psi / c^2$ in the pitch-angle scattering term, which relates our distribution function to one defined in terms of time and position in the local solar wind frame (Webb & Gleeson 1979; see also the scattering terms of Skilling 1975, Earl 1984). Then replacing $\Delta z / \Delta t$, $\Delta \mu / \Delta t$, and $\Delta p / \Delta t$ with \dot{z} , $\dot{\mu}$, and \dot{p} from equations (7), (8), and (10), we derive the following transport equation:

$$\begin{aligned} \frac{\partial F(t, \mu, z, p)}{\partial t} = & - \frac{\partial}{\partial z} \mu v F(t, \mu, z, p) && \text{(streaming)} \\ & - \frac{\partial}{\partial z} \left(1 - \mu^2 \frac{v^2}{c^2} \right) v_{\text{sw}} \sec \psi F(t, \mu, z, p) && \text{(convection)} \\ & - \frac{\partial}{\partial \mu} \frac{v}{2L(z)} \left[1 + \mu \frac{v_{\text{sw}}}{v} \sec \psi - \mu \frac{v_{\text{sw}} v}{c^2} \sec \psi \right] \\ & \cdot (1 - \mu^2) F(t, \mu, z, p) && \text{(focusing)} \\ & + \frac{\partial}{\partial \mu} v_{\text{sw}} \left(\cos \psi \frac{d}{dr} \sec \psi \right) \mu (1 - \mu^2) \\ & \cdot F(t, \mu, z, p) && \text{(differential convection)} \\ & + \frac{\partial}{\partial \mu} \frac{\varphi(\mu)}{2} \frac{\partial}{\partial \mu} \left(1 - \mu \frac{v_{\text{sw}} v}{c^2} \sec \psi \right) F(t, \mu, z, p) && \text{(scattering)} \\ & + \frac{\partial}{\partial p} p v_{\text{sw}} \left[\frac{\sec \psi}{2L(z)} (1 - \mu^2) + \cos \psi \frac{d}{dr} \sec \psi \mu^2 \right] \\ & \cdot F(t, \mu, z, p). && \text{(deceleration)} \end{aligned} \quad (11)$$

The numerical code can accommodate any desired functional form for the angle between the field line and the radial direction, $\psi(z)$, the focusing length, $L(z)$, and the pitch-angle scattering coefficient, $\varphi(\mu)$. In this work, we use the Archimedean field model of Parker (1958) with $b = 0$, so that

$$\begin{aligned}\cos \psi &= \frac{R}{\sqrt{r^2 + R^2}} \\ L &= \frac{r(r^2 + R^2)^{3/2}}{R(r^2 + 2R^2)},\end{aligned}$$

where $R = v_{\text{sw}}/\Omega \sin \theta$, Ω is the angular rotation rate of the sun, and the radius is in turn a function of z .

We also use

$$\varphi(\mu) = A|\mu|^{q-1}(1 - \mu^2), \quad (12)$$

which was derived in the context of quasilinear scattering theory (Jokipii 1971; Earl 1973), and is adopted here as a convenient and commonly understood parameterization of the pitch-angle scattering. Some care is required when using equation (12), because of the singularity at $\mu = 0$. In particular, when using a finite difference method to numerically solve the transport equation, Ng & Wong (1979) used an effective scattering coefficient given (in our notation) by

$$\varphi_{\text{eff}}(\mu) = \frac{v}{2L(z)}(1 - \mu^2) \frac{\Delta\mu}{\tanh\left\{\frac{v}{2AL(z)}[I(\mu + \Delta\mu/2) - I(\mu - \Delta\mu/2)]\right\}},$$

where

$$I(\mu) \equiv \text{sgn}(\mu) \frac{|\mu|^{2-q}}{2-q}.$$

and $\Delta\mu$ is the grid spacing in the μ coordinate. Although Ng and Wong only used this form for μ near zero, we use it for all values of μ , noting that $\varphi_{\text{eff}}(\mu) \rightarrow \varphi(\mu)$ when $\mu \gg \Delta\mu$. By using $\varphi_{\text{eff}}(\mu)$, we achieve a great improvement in the accuracy of the numerical solutions.

Finally, it is convenient to describe the pitch-angle scattering in terms of a spatial mean free path, λ , given by

$$\lambda \equiv \frac{3D}{v},$$

where D is a spatial diffusion coefficient. Considering pitch-angle scattering alone, one can derive a diffusion coefficient of

$$D = \frac{v^2}{4} \int_{-1}^1 \frac{(1 - \mu^2)^2}{\varphi(\mu)} d\mu$$

(Jokipii 1968, Hasselmann & Wibberenz 1968). If we replace the continuous variable μ with a discrete set of grid points, the actual diffusion coefficient in the simulation is given by

$$D = \frac{v^2}{4} \sum_{\mu} \frac{(1 - \mu^2)^2}{\varphi_{\text{eff}}(\mu)} \Delta\mu,$$

where the sum is over μ values halfway between grid points, and $\varphi_{\text{eff}}(\mu)$ is calculated in the limit of no focusing. We then find the scattering amplitude, A , that is needed to generate the desired mean free path.

The transport equation presented here is different from those generally used to model solar modulation (Jokipii 1992) in that the distribution function depends on the pitch angle, in addition to the position and momentum. Therefore, this framework can be used to study anisotropic distributions of galactic cosmic rays subject to solar modulation.

This transport equation can be shown to be equivalent to a special case of the transport equation derived by Skilling (1975), with the Alfvén speed set to zero and the solar wind speed set to v_{sw}^c .

The essential difference between the present derivation and that of Luhmann (1976) is that the latter derivation was performed in the fixed frame. Scattering due to fluctuations moving at a fixed speed was then expressed by four terms involving the diffusion coefficients, $D_{\mu\mu}$, $D_{\mu p} = D_{p\mu}$, and D_{pp} (see also Schlickeiser 1989). It is important to note that these four terms mathematically conspire to act as the single scattering term in equation (11) (Earl 1984). In fact, when viewed in the local solar wind frame, where the magnetic fluctuations are fixed, scattering conserves the momentum, so the D_{pp} term of Luhmann (1976) only arises upon transformation to the fixed frame (see Figure 1). For a numerical solution, it would be difficult to evaluate the four diffusion terms properly so that they would behave as the single term in equation (11), and errors in the apparent p -diffusion would probably dominate the true deceleration.

3. NUMERICAL METHOD

The above transport equation was solved directly by means of a finite-difference method. The method was adapted from that of Ruffolo (1991), but many modifications were needed to accommodate adiabatic deceleration and other effects of the solar wind. In particular, the distribution function must now be computed for various values of the momentum, p . In order to avoid a great increase in the computer time required, the numerical code was designed to provide accurate results even for widely spaced values of p . Thus while $F(t, \mu, z, p)$ is calculated for an evenly spaced grid of (t, μ, z) coordinates, values of p can be chosen according to the user's convenience, e.g., corresponding to momenta for which experimental data are reported.

When solving equation (11), we need to specify boundary conditions at the edges of the (t, μ, z, p) domain. As $\mu \rightarrow \pm 1$, we require the μ -flux,

$$\begin{aligned}
 S_\mu(t, \mu, z, p) = & \left\{ \frac{v}{2L(z)} \left[1 + \mu \frac{v_{\text{sw}}}{v} \sec \psi - \mu \frac{v_{\text{sw}} v}{c^2} \sec \psi \right] (1 - \mu^2) \right. \\
 & \left. - v_{\text{sw}} \left(\cos \psi \frac{d}{dr} \sec \psi \right) \mu (1 - \mu^2) \right\} F(t, \mu, z, p) \\
 & - \frac{\varphi(\mu)}{2} \frac{\partial}{\partial \mu} \left(1 - \mu \frac{v_{\text{sw}} v}{c^2} \sec \psi \right) F(t, \mu, z, p), \tag{13}
 \end{aligned}$$

to vanish so that no particles “flow” to the non-physical regions where $|\mu| > 1$; this is satisfied by the terms including the factor $(1 - \mu^2)$, and by our choice for the scattering coefficient, $\varphi(\mu)$. Other boundary conditions can be adapted to the problem at hand. For simulations of the transport of particles coming directly from a solar flare, the initial distribution function, $F(t, \mu, z, p)|_{t=0}$ (where t is set to zero at the time of the flare), is only non-zero near $z = 0$, i.e., near the sun. At the z -boundaries, we allow particles to flow out and set the influx to zero, that is, particles are absorbed at the boundaries. In practice, the outer z -boundary can be set sufficiently far from the sun that it has no effect on the distribution of particles at the point of interest during the course of the simulation, and the inner z -boundary near the Sun has only a small effect, because intense focusing there reflects most incoming particles before they reach the boundary (Ng & Wong 1981). Finally, the distribution function vs. momentum at a fixed $s = vt$ is assumed to fall off as $p^{-\delta}$ above the highest simulated value of p (see discussion below). This is equivalent to fixing the p -flux at the upper p -boundary.

We solve the transport equation by applying a technique known as operator splitting, in which $F(t, \mu, z, p)$ is sequentially updated according to individual terms or groups of terms on the right-hand side of equation (11). The procedure can be physically interpreted as having particles alternately undergo changes in μ , p , and z during each time step. As the time step is shortened, this sequence provides a more accurate approximation to the simultaneous action of these processes. The resulting procedure for updating $F(t, \mu, z, p)$ from t to $t + \Delta t$ is as follows (in equations with a left-pointing arrow, the terms on the left hand side refer to updated values):

1. Update the distribution function with half the effect of pitch-angle scattering, focusing, and differential convection, i.e., processes which affect μ . Step 4 accounts for the second half; the treatment of these processes both before and after steps 2 and 3 improves the convergence of the method. For fixed values of z and p , the μ -flux, S_μ , is evaluated between each pair of neighboring grid points, μ and $\mu + \Delta\mu$. Using equation (13) and the finite difference approximation for derivatives, we obtain

$$\begin{aligned}
 S_\mu(\bar{\mu}) \approx & \left\{ \frac{v}{2L(z)} \left[1 + \bar{\mu} \frac{v_{\text{sw}}}{v} \sec \psi - \bar{\mu} \frac{v_{\text{sw}} v}{c^2} \sec \psi \right] \right. \\
 & \left. - v_{\text{sw}} \left(\cos \psi \frac{d}{dr} \sec \psi \right) \bar{\mu} \right\} \\
 & \cdot (1 - \bar{\mu}^2) \left[\frac{F(\mu + \Delta\mu) + F(\mu)}{2} \right] \\
 & - \frac{\varphi_{\text{eff}}(\bar{\mu})}{2} \left[\frac{F'(\mu + \Delta\mu) - F'(\mu)}{\Delta\mu} \right],
 \end{aligned}$$

where $\bar{\mu} \equiv \mu + \Delta\mu/2$ and $F' = (E'/E)F = (1 - \mu v v_{\text{sw}} \sec \psi / c^2)F$. The μ -flux can be calculated using f at the start of the step (explicitly), at the end of the step (implicitly), or alternately explicitly and implicitly for better stability and accuracy (Crank & Nicolson 1947). Using the last approach, the code first solves the coupled explicit equations,

$$F(\mu) \leftarrow F(\mu) - \left(\frac{\Delta t}{4n}\right) \left[\frac{S_\mu(\mu + \Delta\mu/2) - S_\mu(\mu - \Delta\mu/2)}{\Delta\mu} \right],$$

for each grid point, μ , then solves the implicit equations,

$$F(\mu) + \left(\frac{\Delta t}{4n}\right) \left[\frac{S_\mu(\mu + \Delta\mu/2) - S_\mu(\mu - \Delta\mu/2)}{\Delta\mu} \right] \leftarrow F(t, \mu),$$

and repeats the process for a total of n explicit and n implicit substeps. Each substep represents a time increment of $\Delta t/(4n)$, so these $2n$ steps account for scattering and focusing over half of Δt . The number, n , is repeatedly doubled until the resulting flux changes by less than the preset absolute tolerance or the preset relative tolerance.

2. Update the distribution function with the effect of deceleration, i.e., the systematic decrease in p . This step requires particular care, so that numerical errors do not dwarf the small effect of deceleration. Since the spacing between p -grid points is typically much larger than the change in momentum during a single time step, it is necessary to interpolate the distribution function between p -grid points.

To minimize the error of this approximation, the interpolation should be between p -grid points at the same time, t , or at the same “distance traveled,” $s = vt$, depending on the physical situation. For example, consider the distribution of particles after a solar flare. For two neighboring values of the momentum, p_1 and p_2 , where $p_1 < p_2$, the μ - z distributions will evolve differently vs. t , because the particles at p_2 move faster than those at p_1 . However, their evolution vs. $s = vt$ is quite similar. Thus geometric interpolation at a constant s provides an accurate estimate of the distribution function at intermediate p values. In contrast, interpolation at a constant t is inaccurate, and can also introduce an erroneous, non-zero flux of particles well beyond a distance vt from the sun. Therefore, interpolation at constant s is more appropriate for modeling the transport of solar flare particles; interpolation at constant t would be more appropriate for certain other astrophysical situations.

The transport equation for deceleration alone can be written as

$$\frac{\partial}{\partial t} F(t, \mu, z, p) = \frac{1}{\tau_d} \frac{\partial}{\partial p} p F(t, \mu, z, p),$$

where the deceleration time, τ_d , is given by

$$\frac{1}{\tau_d} = v_{\text{sw}} \left[\frac{\sec \psi}{2L(z)} (1 - \mu^2) + \cos \psi \frac{d}{dr} \sec \psi \mu^2 \right]. \quad (14)$$

This in turn gives us

$$\frac{\partial}{\partial t} p F(t, \mu, z, p) = \frac{1}{\tau_d} \frac{\partial}{\partial \ln(p/p_0)} p F(t, \mu, z, p),$$

for a fixed reference momentum p_0 , which has the solution

$$p F(t + \Delta t, \mu, z, p) = p e^{\Delta t/\tau_d} F(t, \mu, z, p e^{\Delta t/\tau_d}). \quad (15)$$

When the interpolation is performed at a constant t , this formula can be used directly. When interpolating at a constant s , we note that the product pF is constant along characteristics, which are straight lines of slope $-1/\tau_d$ on a semi-logarithmic graph of p vs. t (see Fig. 4). We then find the intersection between the curve of constant s passing through the grid point (t_i, p_j) and the characteristic passing through (t_{i+1}, p_j) , where $t_{i+1} = t_i + \Delta t$. At this characteristic-intersection point, (t^*, p^*) , the distribution function is calculated by geometric interpolation between $F(p_j)$ and $F(p_{j+1})$ at the next higher p -grid point (or for the highest p -grid point, by assuming that $F \propto p^{-\delta}$ for a constant δ lines of constant s). We then use

$$pF(t_{i+1}, \mu, z, p_j) = p^*F(t^*, \mu, z, p^*)$$

to calculate the new value of the distribution function.

Note that we are free to choose a different value of Δt for each value of p . We therefore set $\Delta t = \Delta s/v$ for a fixed value of Δs , so that F is updated to $s_{i+1} = s_i + \Delta s$ for each p -grid point (see Fig. 4).

This characteristic-intersection method fails when the logarithmic slope of the characteristics, $-1/\tau_d$, is steeper than that of the constant- s curve, $-\gamma^2/t$, or when

$$t > \gamma^2 \tau_d.$$

The deceleration time, τ_d , is at least 5.7 days near the Earth, for an Archimedean field and a solar wind speed of 400 km/s. Thus this code is valid for simulating “well-connected” solar flare events, for which the flare and detector are on nearby magnetic field lines, and the flare event has a short duration; for poorly-connected events, the code would need to be modified to switch to interpolation at constant t for later times, and also to take into account drifts and diffusion perpendicular to the field.

3. Account for streaming and convection in the z -direction. The streaming term alone can be treated (Ruffolo 1991) by simply moving the distribution function from one z -grid point to another:

$$F(i\Delta\mu, z, p) \leftarrow F(i\Delta\mu, z - i\Delta z, p),$$

where i labels the μ -grid points, $\mu = i\Delta\mu$, and $\Delta z = \Delta\mu(v\Delta t)$. This is an exact solution to a transport equation for streaming alone,

$$\frac{\partial F(t, \mu, z, p)}{\partial t} = -\mu v \frac{\partial}{\partial z} F(t, \mu, z, p),$$

and since no finite difference approximation is used, there is no numerical “diffusion”. When convection is included, this approach can be modified by occasionally moving the distribution function forward by an additional step, Δz . Thus numerical diffusion is still absent, i.e., a sharp pulse or gradient in the distribution function can be maintained intact. There is a price to pay for the elimination of numerical diffusion: because the convection speed, $(1 - \mu^2 v^2/c^2)v_{sw} \sec \psi(z)$, is not constant with respect to z , “holes” where $F = 0$ can appear in the μ - z plane. Fortunately, these holes are rapidly filled in by pitch-angle scattering (in steps 1 and 4), and on average the distribution is rarefied in the proper manner. For this reason, the results presented here are averaged over a set of nearby z -grid points.

4. Repeat step 1, updating the pitch-angle distribution for the second half of the scattering, focusing, and differential convection effects. The result of this step is $F(t + \Delta t, \mu, z, p)$.

Starting with the initial condition, $F(0, \mu, z, p)$, we repeat this procedure for each time step, Δt , to generate the particle distribution function for all times of interest.

4. NUMERICAL SIMULATIONS

Several simulations were performed to test the accuracy of the new computer code. For example, when $F \propto p^{-\delta}$ and only the deceleration step is enabled, an exponential decay in the flux was observed, with the proper time constant as given by equation (14). Simulation results for $v_{\text{sw}} = 0$ matched those of the code used in Ruffolo (1991), in which solar wind effects were not included. That code, in turn, successfully fit the observed intensity and pitch-angle distribution vs. time for neutron-decay protons from the solar flare events of 3 June 1982 and 25 April 1984. It has also been tested against the codes of Ng & Wong (1979), Bieber et al. (1980), and more recently, against those of Earl (1987) and Pauls & Burger (1993), as described by Earl et al. (1994).

The remainder of this section describes sample simulations of the transport of solar flare protons. As described earlier, the momentum, p , and the pitch-angle cosine, μ , are defined in the local solar wind frame; quantities in the fixed frame can be derived by a Compton-Getting transformation. The simulations were performed for five momentum values corresponding to kinetic energies of 2, 6, 20, 60, and 200 MeV. The initial condition is that protons are concentrated near the sun. For demonstration purposes, the initial distribution is proportional to p^{-5} ; this is somewhat steep, but not unusual for solar flare protons (see, e.g., Evenson et al. 1984). The initial distribution is concentrated at the highest μ -grid point, because strong focusing near the sun herds the particles into the forward direction, and the normalization is such that the integral of F over μ and z for a kinetic energy of 2 MeV is equal to one. For other parameters, typical values were chosen: the solar wind speed is 400 km/s, and the scattering parameter q and the mean free path λ are 1.5 and 0.3 AU, respectively, for all values of p , z , and t . The step size, $\Delta s = v\Delta t$, is 0.005 AU up to $s = 0.5$ AU, 0.01 AU up to $s = 1$ AU, etc. The μ -grid spacing, $\Delta\mu$, is $2/25$ (i.e., for 25 values of μ), and Δz is set equal to $\Delta s\Delta\mu$ in order to accurately evaluate the streaming term (see §3), i.e., Δz is 4×10^{-4} AU up to $s = 0.5$ AU, 8×10^{-4} AU up to $s = 1$ AU, etc. A typical simulation required approximately 2.5 hours of CPU time on an IBM RISC/6000 computer.

The distribution of 2 MeV protons vs. μ and z is shown in Fig. 5 for different values of $s = vt$, the distance traveled by the protons since the occurrence of the flare, or their maximum possible distance from the sun in the absence of convection. Panels a-d show results for s values of 0.5, 1, 2, and 4 AU, respectively. The general features are typical of focused transport. The protons are initially concentrated in a coherent pulse (Earl 1976) over a narrow range of z values. The distribution is strongest near $\mu = 1$, for which particles move directly along the magnetic field and away from the sun. The distribution function decreases sharply at $\mu = 0$ (where the pitch angle is 90°), because the scattering coefficient approaches zero as $\mu \rightarrow 0$, which inhibits scattering to $\mu < 0$ (see eq. [12]).

Note that for each of the plots in Fig. 5, the right boundary is at $z = s = vt$. Since this is the maximum possible distance from the sun, in the absence of convection, the protons would reach the right edge of the plots if they traveled directly along the field, with $\mu = 1$. In fact, the pulse moves somewhat slower than v because the protons are distributed over a range of μ values. Furthermore, a comparison of panels a-c shows that the pulse moves progressively more slowly. This is because the effect of focusing, which is proportional to the logarithmic gradient of B , becomes weaker as the pulse moves farther from the sun, allowing the average μ to decrease. Later on, when $s = 1.0$ (panel c), much of the pulse has spread to $\mu < 0$; from this point on, the distribution is dominated by a nearly Gaussian “wake” (Earl 1976) that gradually spreads in z as the coherent pulse fades away.

To isolate the effect of the solar wind, simulations were also performed with the solar wind velocity set to zero. The difference, ΔF , between F for $v_{\text{sw}} = 400$ km/s and F for $v_{\text{sw}} = 0$ is displayed in panels e-h of Fig. 5. In each case, the difference is negative behind the pulse, and positive at the leading edge. This can be explained by the effects of solar wind convection and adiabatic deceleration. For small s , convection displaces the narrow pulse by a distance comparable to its width, yielding the bipolar distribution of panel e. Later on, deceleration has a greater cumulative effect, causing a systematic decrease in F (see panel h). Note that each plot of ΔF is drawn to the same scale as the corresponding plot of F , so for this case the solar wind has a substantial impact on the cosmic ray distribution.

The simulated intensity vs. the distance traveled, s , is shown in Fig. 6, both with and without the effect of the solar wind. The intensity shown here is the directional average of the distribution function, F , for fixed values of z and p . The basic features of a rapid rise and a slow decay of the intensity are characteristic of observed solar cosmic-ray distributions after a flare event (in the absence of interplanetary shock effects)

and are in qualitative agreement with the results of the older, diffusive propagation model (e.g., Wibberenz et al. 1989). Since we have assumed that the scattering mean free path, λ , is independent of energy, the evolution of the intensity vs. s is also energy independent in the absence of solar wind effects. Thus the points for $v_{\text{sw}} = 0$ (pluses) for different energies differ by a constant logarithmic offset, and any energy dependence of the intensity evolution for $v_{\text{sw}} = 400$ km/s (solid circles) is due to the effect of the solar wind. For kinetic energies of 60 and 200 MeV, the two sets of points are nearly coincident, indicating that the solar wind has only a small effect on the transport of higher-energy solar cosmic rays; this is because the solar-wind dependent terms in $\partial F/\partial s$ depend on the ratio v_{sw}/v , which is small for higher energy particles. In contrast, there is a significant difference for the lower energies, mainly due to the effect of solar wind convection at early times and of adiabatic deceleration at later times.

One possible diagnostic of the evolution of the intensity of solar cosmic rays is its decay at late times, which typically appears as a straight line on a semi-logarithmic plot. The slope can then be related to λ , the mean free path of interplanetary scattering, based on a model of the interplanetary transport. Our results show that such models should take adiabatic deceleration into account for kinetic energies on the order of 20 MeV or below, or else the derived value of λ will be in error. To quantify this error, let the ‘‘apparent’’ mean free path, λ_a , be defined as the value needed for a simulation with no solar wind to match the late-time decay slope of a simulation for the true λ that includes solar wind effects. Table 1 shows values of λ_a , where the true λ is 0.3 AU. Results are shown both for a spectral index, δ , of 5 as before, and for a more typical case of $\delta = 2.5$. Note that for three cases (including 2 and 6 MeV protons shown in Fig. 6), no reasonable value of λ_a can generate such a steep slope; for $\lambda_a > 0.5$ AU, the decay phase starts after $s = 4$ AU. In determining λ from observational data, it is possible to achieve an accuracy as good as 20% (Ruffolo 1991), but Table 1 shows that for most cases, the error in neglecting deceleration would be greater than this. Even for the rather high energy of 20 MeV, the mean free path would be overestimated by 63% for a flare with a spectral index of 5.

Returning to other results, simulated pitch angle distributions of 2 MeV protons are shown in Fig. 7 for selected s values. For both $r = 0.3$ AU and $r = 1.0$ AU, the pitch-angle distributions before or at the time of the peak flux are highly anisotropic in the forward direction (outward along the magnetic field, or to the right in Fig. 7), which reflects the highly collimated nature of the coherent pulse. At the other extreme, the distributions for late times are nearly isotropic. For intermediate values of s , on the trailing edge of the pulse, more unusual shapes are found, as shown here for $s = 0.6$ AU and $s = 2.52$ AU. Since the trailing edge comprises protons traveling slightly slower than those at the pulse peak, the intensity there is highest at a μ value intermediate between 0 and 1. Note also the sharp gradient at $\mu = 0$, due to the drop in the scattering coefficient as discussed earlier. More examples of such distributions can be found in Bieber et al. (1980).

Finally, we have performed simulations which examine the effects of individual, solar-wind dependent terms in the transport equation. These include terms affecting \dot{p} (deceleration), \dot{z} (convection), and $\dot{\mu}$ (differential convection and corrections to focusing). We ran simulations where one of these factors was included, and the other two were disabled. The terms affecting $\dot{\mu}$ were found to have a very small effect, so we concentrate on the deceleration and convection terms. Fig. 8 shows results for $\delta = 5$, $v_{\text{sw}} = 400$ km/s, $T = 2$ MeV, and $r = 1$ AU, with 1) no solar wind effects, 2) convection only, 3) deceleration only, and 4) all solar wind effects. The main effect of convection is to speed up the pulse, so that protons start to arrive sooner. At later times, convection leads to a slightly steeper decay slope, because the peak in the distribution is convected farther from the point of observation, and because of the rarefaction due to the increase in the convection speed with increasing z . Deceleration creates a widening deficit in the intensity vs. s , and accounts for most of the change in the decay slope upon the inclusion of solar wind effects. Finally, the simulation including all effects exhibits both an earlier rise and a steeper decay at late times.

Fig. 8 seems to indicate an additive relationship between the slope changes due to different effects, which has been employed by previous authors (e.g., Murray et al. 1971). Combining all significant effects, we can express the rate of decay of the intensity vs. s as

$$\frac{1}{vT} \approx \frac{1}{vT_{\text{ssf}}} + \frac{1}{vT_{\text{d}}} + \frac{1}{vT_{\text{c}}},$$

where T_{ssf} is the exponential-decay time constant for streaming, scattering, and focusing, i.e., in the absence of solar wind effects, T_{d} is that due to including deceleration, and T_{c} is that due to including solar wind

convection. These four terms, as derived from the simulations shown in Fig. 8, adding one process at a time, are 0.2480, 0.1327, 0.0871, and 0.0345 AU⁻¹, respectively, so the above approximation is in error by 0.0063 AU⁻¹ (due to interactions between the effects of deceleration and convection). The derived intensity-decay times are then $T = 0.3572$ days, $T_{\text{ssf}} = 0.6676$ days, $T_{\text{d}} = 1.017$ days, and $T_{\text{c}} = 2.57$ days.

It is instructive to compare the above decay time for deceleration with estimates based on a hypothetical transport equation with deceleration alone. From equation (15), we find that the momentum-decay rate, τ_{d} , leads to an intensity-decay time of $\tau_{\text{d}}/(\delta - 1)$ due to the advection of F from higher momenta. For a nearly isotropic pitch-angle distribution at late times, we expect that

$$\frac{1}{\tau_{\text{d}}} = \frac{2}{3} \frac{v_{\text{sw}}}{r},$$

and for $r = 1.0$ AU, $\tau_{\text{d}} = 6.49$ days. The effective value of δ is actually 4.65, due to the enhanced decay of the lower-energy flux. Thus we might expect that the intensity-decay time due to including deceleration would be $T_{\text{d}} = 1.78$ days; however, this is 75% longer than the value observed from the simulations.

A careful examination of the operation of the code shows that step 2 (see §3) generates a decay in the intensity at the expected rate. However, the other steps produce a faster decay when deceleration is included, because of the cumulative effect on the shape of the distribution function. During this late-time, diffusive régime, the processes of streaming and scattering behave as a spatial diffusion process, yielding a diffusive decay rate proportional to $\partial^2 F / \partial z^2$. Because the rate of deceleration is spatially non-uniform, it turns out that deceleration for $s < 4.0$ AU increases the magnitude of the diffusive decay rate in the neighborhood of $r = 1.0$ AU. By this means, the influence of deceleration on the intensity decay is effectively enhanced by 75% over that due to momentum advection alone.

5. DISCUSSION AND CONCLUSIONS

The results of the preceding section justify the consideration of adiabatic deceleration in focused transport models. One might expect that the effect of deceleration could be estimated from equation (15), and that this estimated decay rate could be simply added to that due to the other processes (e.g., Murray et al., 1971). However, we have shown that the effect of including deceleration can be much greater than the simple estimate, because the effect is greatly amplified by an interaction with diffusive processes. The magnitude of amplification depends on the cumulative effect of deceleration on the shape of the distribution function, F , which in turn depends on the detailed history of the distribution function. Thus to accurately evaluate the effect of deceleration on the transport of solar cosmic rays, it is necessary to fully incorporate the process into a numerical code for focused transport, as we have done here.

We have also pointed out possible errors due to neglecting deceleration in the determination of the mean free path, λ , from the late-time intensity decay rate, for various kinetic energies and two values of the spectral index. This naturally leads to the question of how λ would be affected by other processes which have been neglected. The most important of these are diffusion and drifts perpendicular to the magnetic field. A very rough estimate shows that these effects are of the same order of magnitude as adiabatic deceleration, so these are important processes which should be taken into account. [Note, however, the justification for their neglect in Ng (1987).] Efforts in this direction have been hampered by unresolved issues, such as the magnitude of the diffusion coefficient, whether perpendicular spreading occurs more in the interplanetary medium (as diffusion) or in the corona, over what distance or speed coronal propagation takes place, etc. In certain flare events, a strong interplanetary shock is generated, and there are various mechanisms by which particles can be accelerated or their transport can be affected [see Jones (1990) for a relevant transport equation]. Other conceivable effects on the particles, such as centripetal or Coriolis acceleration in the corotating frame, can be shown to be orders of magnitude smaller.

In addition to the late-time decay slope, one can also make use of other aspects of the simulation results to fit observed intensity and pitch-angle distributions. The simulation results could serve as templates or response functions for an impulsive injection of particles, so that the time dependence of the injection can be adjusted to fit the observations (see Ma Sung & Earl 1978; since perpendicular diffusion in the interplanetary medium is neglected, this is tantamount to assuming that all perpendicular motion takes place in the solar corona). Note that the effect of convection is also important (see Figure 8), especially in regard to the

timing of the pulse's arrival, which provides the most sensitive information about the time dependence of the injection (Ruffolo 1991).

Other applications of this numerical method can be envisioned. It could be applied to various situations in which adiabatic deceleration or solar wind effects are known to play a major role in cosmic ray transport, such as Forbush decreases, shock acceleration, or solar modulation. Since the key feature of this work is the simultaneous treatment of transport in position, momentum, and pitch angle, the method would most useful when there is a significant anisotropy in the directional distribution; otherwise, existing numerical or analytic methods would suffice.

In summary, we have re-examined the first-order effects of the solar wind on cosmic-ray transport, including convection, deceleration, and pitch-angle effects, from the point of view of focused transport theory. These effects are then incorporated into a numerical code for simulating the distribution of energetic particles as a function of time, pitch angle, position, and momentum. This is used to model the transport of solar flare protons, and it is found that both convection and deceleration have a significant impact on the evolution of the distribution. In particular, the influence of deceleration is greatly enhanced by interactions with the other processes. In addition, this numerical method is expected to be applicable to a variety of situations where solar wind and pitch-angle dependent effects must be evaluated simultaneously.

The author would like to thank Steve Arendt, John Bieber, Jim Earl, Paul Evenson, Peter Meyer, and Eugene Parker for valuable discussions regarding this work. Special thanks go to Chee Ng for his detailed comments as a referee for this article. I am grateful to Burin Asavapibhop, Pisit Lilapattana, Wantana Songprakob, and Montien Tienpratip for programming work. Finally, I would like to thank the Laboratory for Astrophysics and Space Research at the University of Chicago for kindly allowing remote access to their computing facilities.

REFERENCES

- Bieber, J. W. 1977, Ph.D. thesis, Univ. Maryland
Bieber, J. W., Earl, J. A., Green, G., Kunow, H., Müller-Mellin, R., & Wibberenz, G. 1980, *J. Geophys. Res.*, 85, 2313
Crank, J., & Nicolson, P. 1947, *Proc. Cambridge Phil. Soc.*, 43, 50
Compton, A. H., & Getting, I. A. 1935, *Phys. Rev.*, 2d ser., 47, 817
Dorman, L. I. 1965, *Proc. 9th Internat. Cosmic Ray Conf.*, 1, 292
Earl, J. A. 1973, *ApJ*, 180, 227
_____. 1976, *ApJ*, 205, 900
_____. 1984, *ApJ*, 278, 825
_____. 1987, *Proc. 20th Internat. Cosmic Ray Conf.*, 3, 198
Earl, J. A., Bieber, J. W., Pauls, H. L., & Ruffolo, D. 1994 (in preparation)
Evenson, P., Meyer, P., Yanagita, S., & Forrest, D. J. 1984, *ApJ*, 283, 439
Forman, M. A. 1970, *Planet. Space Sci.*, 18, 25
Gleeson, L. J., & Axford, W. I. 1967, *ApJ*, 149, L115
Hasselmann, K., & Wibberenz, G. 1968, *Zs. Geophysik*, 34, 353
Jokipii, J. R. 1966, *ApJ*, 146, 480
_____. 1968, *ApJ*, 152, 671
_____. 1971, *Rev. Geophys. Space Phys.*, 9, 27
_____. 1992, in *Astronomy and Astrophysics Encyclopedia*, ed. S. P. Maran (New York: Van Nostrand Reinhold; Cambridge: Cambridge Univ. Press), 141
Jokipii, J. R., & Parker, E. N. 1970, *ApJ*, 160, 735
Jones, F. C. 1990, *ApJ*, 361, 162
Kóta, J., Merényi, E., Jokipii, J. R., Kopriva, D. A., Gombosi, T. I., & Owens, A. J. 1982, *ApJ*, 254, 398
Luhmann, J. G. 1976, *J. Geophys. Res.*, 81, 2089
Ma Sung, L. S., & Earl, J. A. 1978, *ApJ*, 222, 1080
Murray, S. S., Stone, E. C., & Vogt, R. E. 1971, *Phys. Rev. Lett.*, 26, 663
Ng, C. K., & Wong, K.-Y. 1979, *Proc. 16th Internat. Cosmic Ray Conf.*, 5, 252
_____. 1981, *Geophys. Res. Lett.*, 8, 113

- Ng, C. K. 1987, *Solar Phys.*, 114, 165
- Parker, E. N. 1958, *ApJ*, 128, 664
- _____. 1965, *Planet. Space Sci.*, 13, 9
- Pauls, L. H., & Burger, R. A. 1993, *Proc. 23rd Internat. Cosmic Ray Conf.*, 3, 191
- Roelof, E. C. 1969, in *Lectures in High Energy Astrophysics*, ed. H. Ogelman & J. R. Wayland (NASA SP-199) (Washington: NASA), 111
- Ruffolo, D. 1991, *ApJ*, 382, 688
- Schlickeiser, R. 1989, *ApJ*, 336, 243
- Singer, S. F. 1958, *Nuovo Cimento, Ser. 10*, 8, Suppl. 2, 334
- Singer, S. F., Laster, H., & Lenchek, A. M. 1962, *J. Phys. Soc. Japan*, 17, Suppl. A-2, 583
- Skilling, J. 1971, *ApJ*, 170, 265
- _____. 1975, *MNRAS*, 172, 557
- Webb, G. M., & Gleeson, L. J. 1979, *Ap&SS*, 60, 335
- Wibberenz, G., Kecskeméty, K., Kunow, H., Somogyi, A., Iwers, B., Logachev, Yu. I., & Stolpovskii, V. G. 1989, *Solar Phys.*, 124, 353

Table 1. Apparent Mean Free Paths

T (MeV)	λ_a (AU) for $\delta = 2.5$	λ_a (AU) for $\delta = 5$
2	... ^a	... ^a
6	0.47	... ^a
20	0.38	0.49
60	0.36	0.40
200	0.34	0.37

^a Change in slope is too great to be fit by a reasonable value of λ_a .

Figure Captions

- Fig. 1. Illustration of the actions of adiabatic focusing and pitch-angle scattering in a) the fixed frame and b) the solar wind frame. Focusing acts to increase v_{\parallel} along lines of constant velocity in the fixed frame, while scattering acts in either direction along lines of constant velocity in the solar wind frame. “S” indicates the velocity of the solar wind frame relative to the fixed frame, and “F” indicates the velocity of the fixed frame relative to the solar wind frame.
- Fig. 2. Schematic trajectory of a cosmic ray particle alternately undergoing scattering and focusing, as viewed in the solar wind frame. The combination of the two processes leads to a systematic deceleration of the particle.
- Fig. 3. Schematic of the average magnetic field (*curved lines*) in the inner solar system, illustrating the definitions of the variables z and ψ for the point of interest (*solid circle near the top of the figure*).
- Fig. 4. Illustration of the characteristic-intersection method for computing the effect of deceleration. The quantity pF is constant along characteristics (*dotted lines*), which are straight lines of constant slope in this semi-logarithmic plot. Solid lines are for constant values of $s = vt$. The value of $F(t_{i+1}, p_j)$ is derived from that at the point of intersection, $F(t^*, p^*)$, which is in turn derived by geometric interpolation between $F(p_j)$ and $F(p_{j+1})$ along a line of constant s .
- Fig. 5. Panels a-d: Distribution, F , of 2 MeV protons vs. the distance along the magnetic field, z , and the pitch-angle cosine, μ , in the solar wind frame for $v_{\text{sw}} = 400$ km/s and a) $s = 0.5$ AU, b) $s = 1$ AU, c) $s = 2$ AU, and d) $s = 4$ AU, where $s = vt$ is the distance traveled. Panels e-h: Difference, ΔF , between distributions for $v_{\text{sw}} = 400$ km/s and $v_{\text{sw}} = 0$ km/s, showing the effects of the solar wind on the protons’ transport for e) $s = 0.5$ AU, f) $s = 1$ AU, g) $s = 2$ AU, and h) $s = 4$ AU. Note that adjacent panels are plotted to the same scale.
- Fig. 6. Simulated intensity vs. distance traveled, s , for radii of 0.3 and 1 AU, kinetic energies of 2, 6, 20, 60, and 200 MeV. Results are shown for solar wind velocities of 0 km/s (+) and 400 km/s (●). Small irregularities in the latter are an artifact of the numerical treatment of solar wind convection (see §3). Squares indicate points for which pitch angle distributions are shown in Fig. 7.
- Fig. 7. Polar plots of the 2 MeV proton intensity vs. pitch angle in the solar wind frame for various values of r and s . Each plot is normalized to the same radius for a pitch angle of zero, which is toward the right in each plot.
- Fig. 8. The logarithm of the intensity of 2 MeV protons vs. distance traveled, s , for simulations that included no solar wind effects (+), convection only (○), deceleration only (×), and all solar wind effects (●), for a radius of 1 AU. Note that convection results in an earlier arrival of protons, and deceleration causes a lower intensity and a faster decay after the peak.

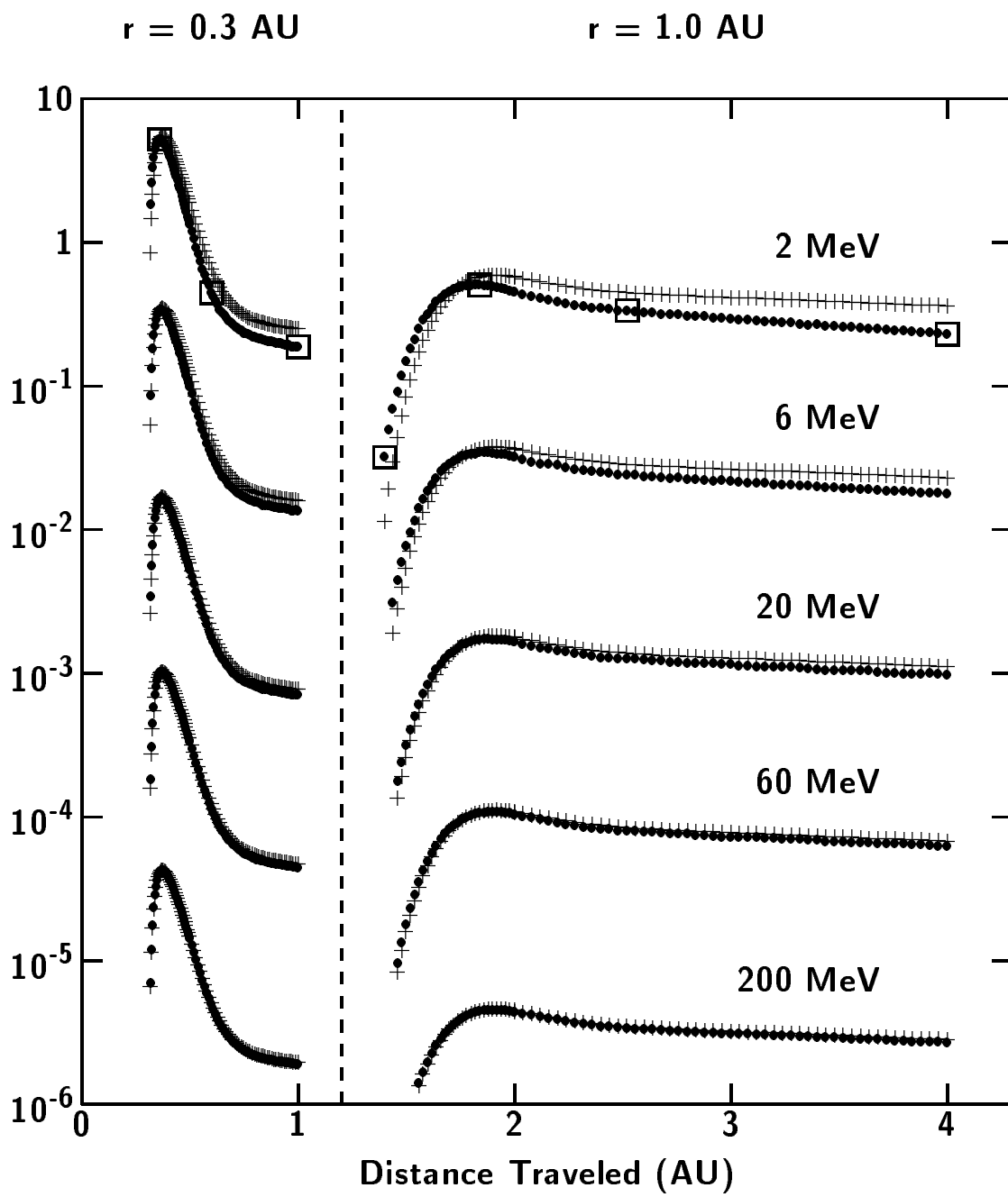


Fig. 6

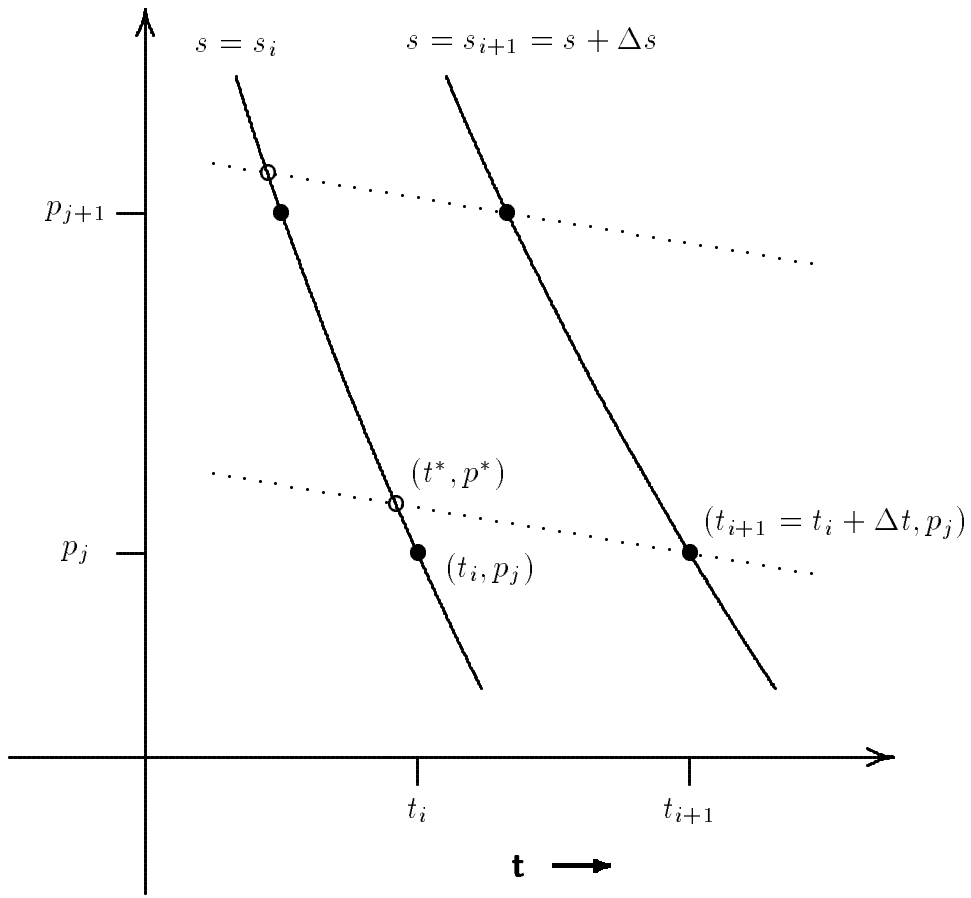


Fig. 4

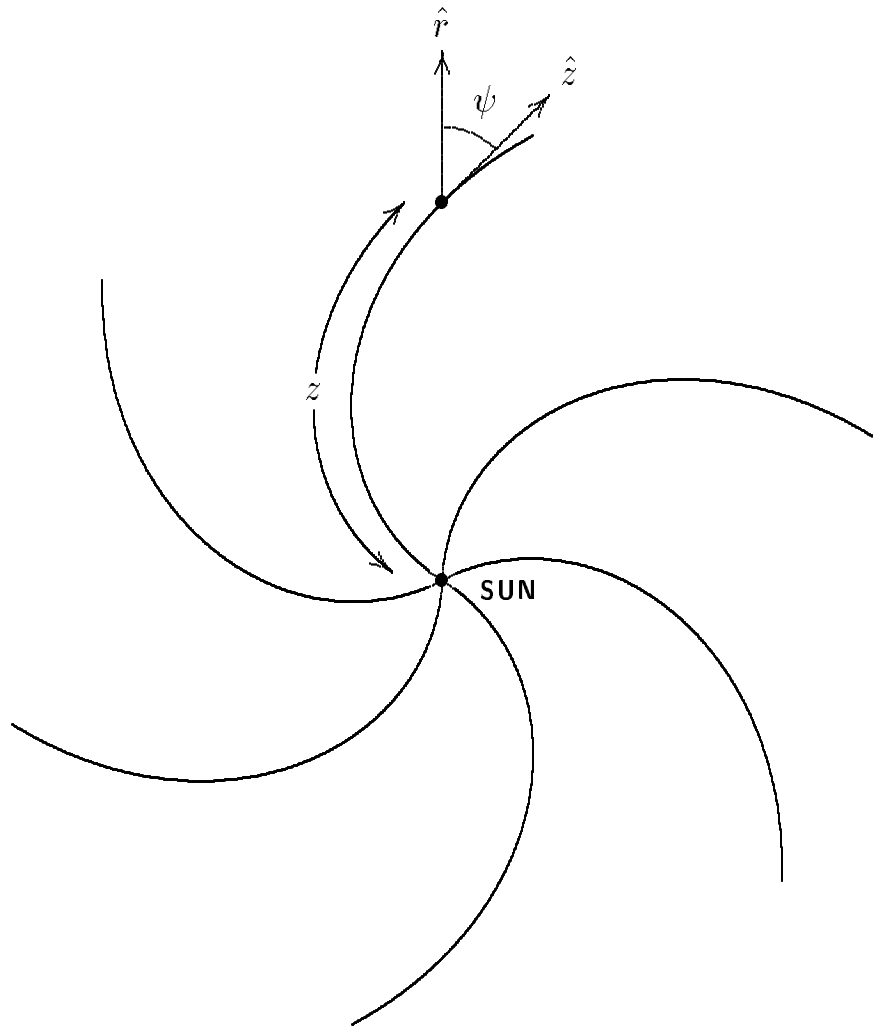


Fig. 3

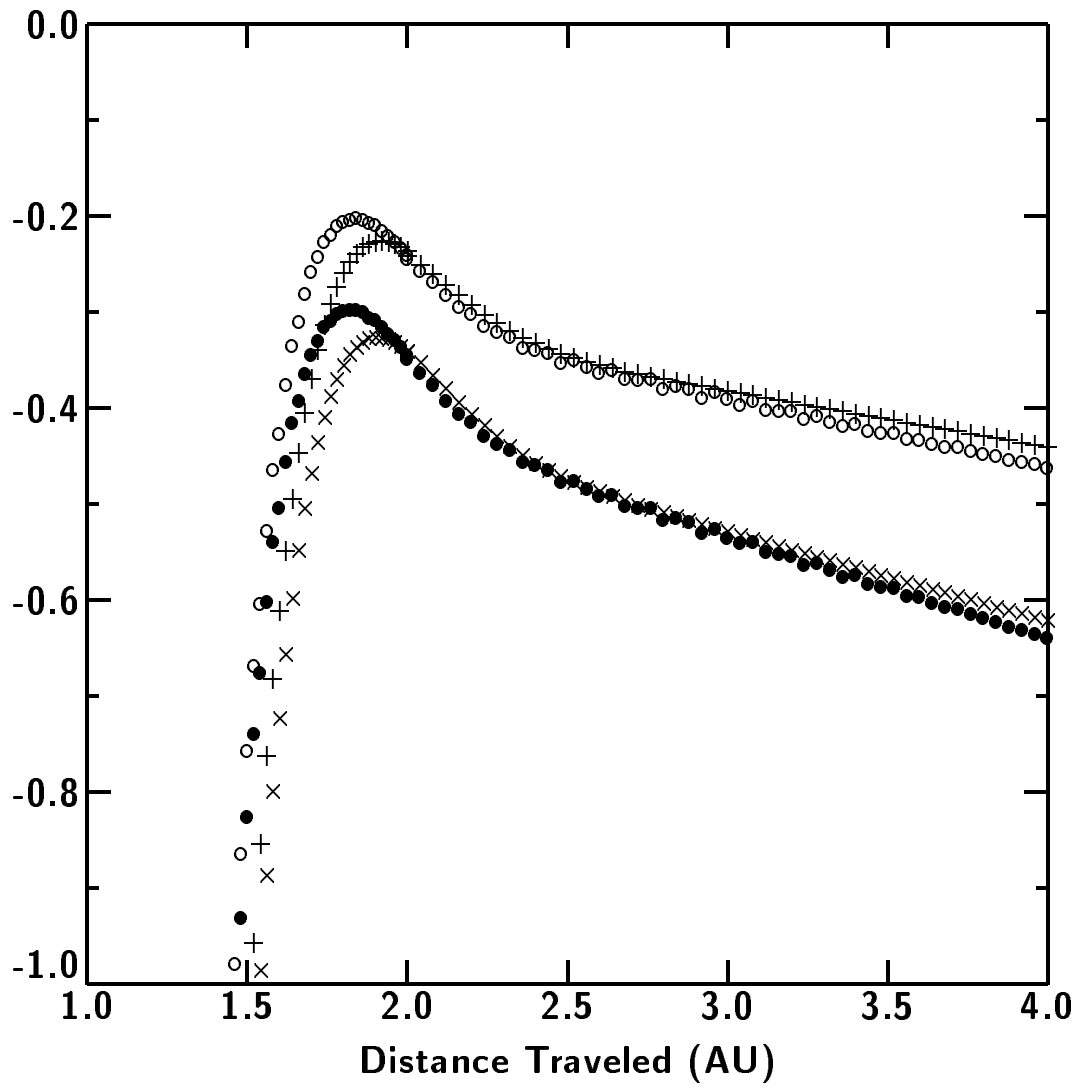


Fig. 8

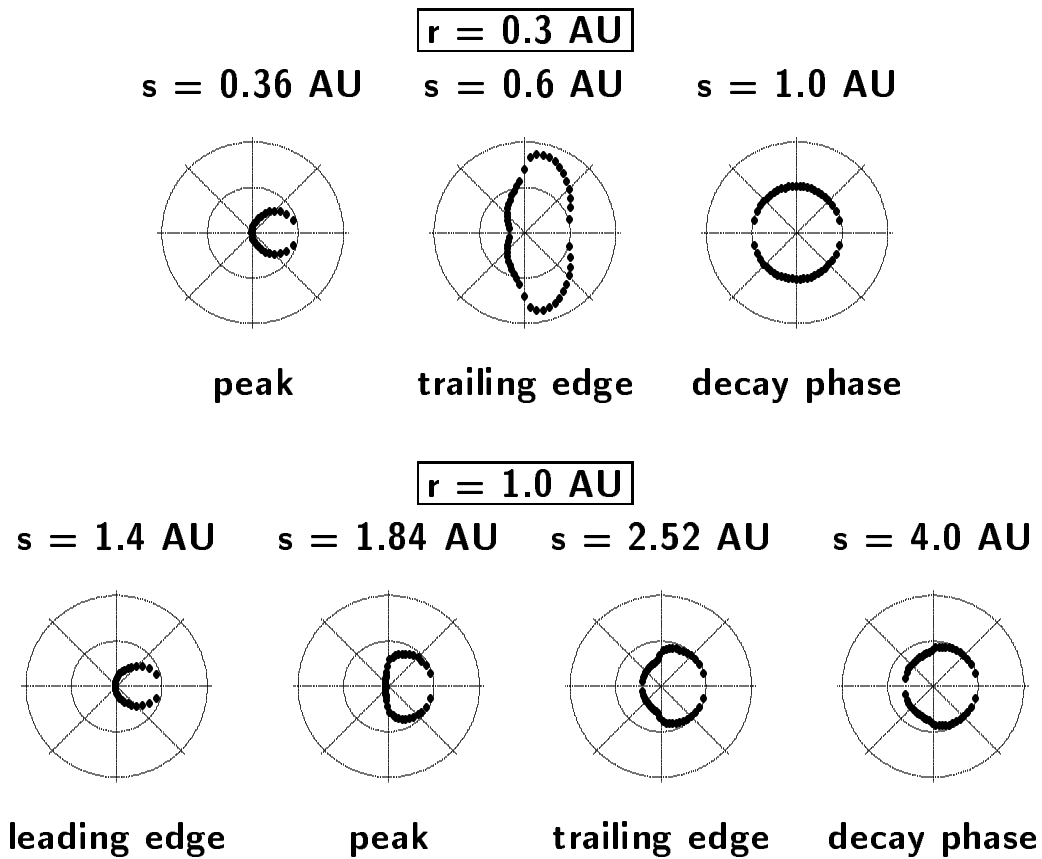


Fig. 7

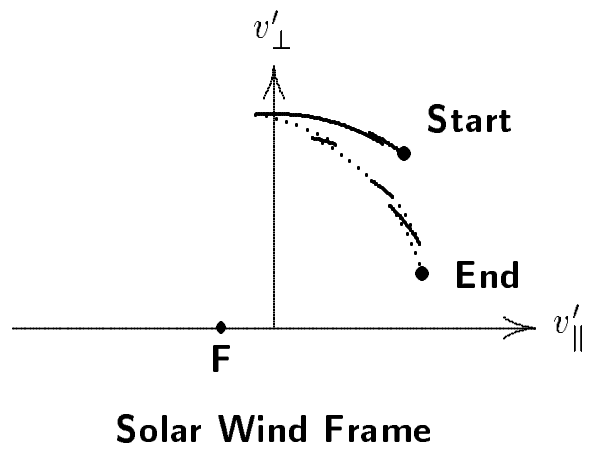
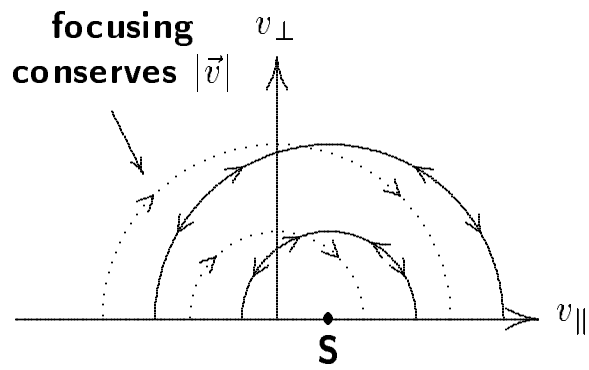


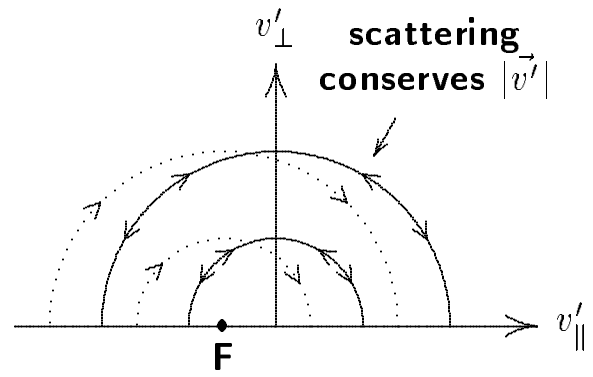
Fig. 2

a



Fixed Frame

b



Solar Wind Frame

Fig. 1